Hindawi
Advances in Materials Science and Engineering
Volume 2018, Article ID 5916180, 12 pages
https://doi.org/10.1155/2018/5916180

Research Article

Adhesion Characteristics of Tire-Asphalt Pavement Interface Based on a Proposed Tire Hydroplaning Model

Binshuang Zheng, Xiaoming Huang, Weiguang Zhang, Runmin Zhao, and Shengze Zhu

School of Transportation, Southeast University, Nanjing 210096, China

Correspondence should be addressed to Xiaoming Huang; huangxm@seu.edu.cn

Received 21 August 2018; Accepted 17 October 2018; Published 31 October 2018

Academic Editor: Ivan Giorgio

In order to study the adhesion between tire and asphalt pavement, we established a finite element model of a hydroplaning, inflatable, patterned tire based on the coupled Eulerian–Lagrangian method and then validated the model's applicability. We numerically calculated tire-pavement adhesion curves for three types of pavement: asphalt concrete (AC), stone mastic asphalt (SMA), and open-graded friction course (OGFC). In accordance with adhesion characteristic theory with regard to tires and asphalt pavements, we analyzed the influential factors that affect the adhesion characteristics of the tire-asphalt pavement interface in an antilock braking system and under damp conditions. The results show that the adhesion between tire and pavement is related to the movement of the tire. In this study, the longitudinal adhesion coefficient for the tire-pavement interface initially increased with an increase in the slip rate and then decreased. Once the slip rate was about 20 percent, the longitudinal adhesion reached its maximum value. In addition, we found that a deep surface macrotexture improved the hydroplaning speed of the tire when the water film was not too thick and the inflation pressure was high. Also, dry pavement led to better adhesion than a wet state in terms of specific mean profile depth. With the same water film thickness, the adhesion coefficient decreased with an increase in driving velocity. The OGFC pavement offered better skid resistance than both AC pavement and SMA pavement.

1. Introduction

Friction between tire and pavement has two distinct force components. As a vehicle moves, the distribution of the vehicle load over the actual contact area is uneven, so the contact area changes constantly. The maximum friction coefficient may occur in any part of the contact area. Therefore, adhesion characteristics should be considered when analyzing tire-pavement contact. Typically, drivers are cautious and drive relatively slowly (i.e., low velocity) when driving on a slippery pavement surface. Under such conditions, the tires are partly in a water-skiing state [1], and due to the reduction in the tire-road contact area and gradual decrease of adhesion, the probability of traffic accidents greatly increases. Analysis of the influential factors that affect tire-asphalt pavement adhesion characteristics under dry and humid conditions can provide a theoretical reference for designing asphalt pavements with better skid resistance and improved vehicle braking behavior during rainy events.

Several researchers have attempted to develop numerical tools for predicting tire-pavement interactions [2]. The influential factors of adhesion and hysteresis should be considered simultaneously when developing a suitable tire-pavement contact model. To determine the mechanisms that determine tire and pavement interactions for different influential factors and under different conditions, researchers have developed many empirical models, half-empirical models, and simplified theoretical models to describe the relationship between longitudinal adhesion and slip rate. For example, with regard to the variability of tire treads and the viscoelastic properties of rubber materials, Jones suggested that classical friction theory should be corrected by considering adhesion characteristics where the tire and the pavement contact each other [3]. Subsequently, Gim developed a steady-state tire model, referred to as the University of Arizona (UA) Gim model. In Gim's UA model, the tire is simplified into a three-dimensional spring, a dynamic equation for the tire-pavement contact is established, and

the critical slip rate is defined. However, for many intermediate variables in the UA model, some limitations were evident when attempting to solve the dimensionless contact area length [4]. In 1970, Dugoff, assuming that the contact area between tire and pavement was rectangular, determined the variation rule of tire longitudinal force with longitudinal slip rate according to the elastic deformation of the contact zone, and the results were in accordance with tests [5]. The LuGre model was first put forward in 1995 to approximate tire and road adhesion characteristics as strain characteristics. Using a large number of elastic bristles, the LuGre model was able to accurately reflect the longitudinal slip performance of the tire and the asphalt pavement [6]. German proposed a typical polynomial model to approximate the relationship between adhesion coefficient and slip ratio of the tire-pavement interface using a simple polynomial function; however, this model cannot be applied when the slip ratio is high [7]. In 1993, the parameters of the Burckhardt model were varied according to pavement condition, which reflected the change in the longitudinal adhesion coefficient under different pavement conditions. This model can estimate and solve unknown parameters according to vehicle measurement information. In 1991, Pacejka [8] first proposed a typical tire semi-empirical model, referred to as the 'magic formula' model. It utilizes a trigonometric function through the standardization of longitudinal force, lateral force, and return torque.

Currently, the use of a finite element model (FEM) is a popular choice to study tire-pavement interactions. In 2003, based on the theory of energy conservation, Ji used an FEM to analyze the influence of partial hydroplaning on the adhesion coefficient [1]. Based on the relationship equation between adhesion coefficient and water film thickness, Ji could deduce the driving speed. Fwa and colleagues [9–12] established a FEM for tire-asphalt pavement interaction, discussed the influential factors of hydroplaning velocity, and found that the change rule of the friction coefficient varied with the thickness of the water film. However, these studies considered the pavement as a smooth flat surface and did not adequately consider the macro- and microtexture of the asphalt pavement. Based on surface fractal theory, Chen tested the stress distribution of tires and found a positive correlation between the average effective stress and the friction coefficient [13]. However, Chen did not consider adhesion characteristics, and the measurement accuracy was unreliable.

The existing theoretical models of tire-pavement adhesion coefficients are mainly simplified steady-state linear models [14] that assume tire deformation is in the linear range when the tire is in contact with the road surface. These models can only reflect the changing trend of the tire adhesion characteristics in terms of the longitudinal slip rate but cannot be used in automotive control analysis. Hence, this paper deduces that the adhesion coefficient curve varies with the slip ratio for different asphalt pavements. In addition, using the simplified tire model as a mechanical element or actual experimental observation, this paper describes the relationship between the adhesion coefficient and the tire slip ratio when friction is produced between the tire and the road pavement. This paper does not include an intensive study of tire-pavement contact mechanisms, so the essential mechanisms of the adhesion coefficient and influential factors of the adhesion coefficients were not obtained. Therefore, an environmentally friendly and time-saving method that can determine the mechanisms of tire-pavement interactions is urgently needed for pavement skid-resistance performance design.

In view of the above research shortcomings, this study further investigated the adhesion characteristics of the tire-asphalt pavement interface by combining the mechanisms of tire and pavement interactions to obtain an adhesion characteristics curve that can describe the stress characteristics of a rolling tire. The results show the impact of the adhesion coefficient on pavement skid resistance.

2. Objectives and Scope of this Study

The objectives and the scope of this study are as follows:

(i) The primary objective of this study is to determine the adhesion characteristics of the tire-asphalt pavement interface and to derive a FEM that uses a liquid surface tracking technique (i.e., volume of fluid, or VOF) to describe the tire hydroplaning phenomenon for different pavements. This study also aims to provide a theoretical reference for the design of skid-resistant asphalt pavement layers and the braking system of a vehicle for rainy weather.

(ii) We selected three types of typical asphalt pavement rutting slabs for study: asphalt concrete (AC), stone mastic asphalt (SMA), and open-graded friction course (OGFC). We obtained pavement texture depth using computed tomography (CT) scanning technology and established a pavement model with macrotexture information and an inflatable patterned tire model in ABAQUS. Based on the coupled Eulerian–Lagrangian (CEL) method, we applied a water flow model to simulate a hydroplaning tire.

(iii) In order to compare the model accuracy and applicability with other models found in the literatures, we verified the hydroplaning FEM using the tire-pavement contact area and tire footprint. We obtained a tire-pavement adhesion coefficient curve and analyzed the effects of the relevant factors such as pavement materials, tire inflation pressure, tire rolling speed, water film thickness, and pavement macrotexture, i.e., the mean profile depth (MPD), on tire-asphalt pavement adhesion characteristics.

3. Tire Hydroplaning Model

3.1. Tire Model. We established a hydroplaning FEM in ABAQUS and conducted hydroplaning analysis using an explicit dynamic analysis module. The 225-40-R18-type radial tire that we adopted as the tire model was treated as a composite structure. The carcass was made from rubber material and cord-rubber composites. We employed the Yeoh model to describe the hyper-elastic mechanical properties of

the rubber material and applied a surface element embedded rebar unit to simulate the reinforcement composites of the belts, inner liner, cap plies, wire ring, etc. We selected the specific material parameters in the Yeoh model, such as the parameters of the tire skeleton material and rib reinforcement material, according to the relevant literature [15].

We utilized an analytical rigid body to form a rim to ensure that the rim was consistent with the center of the tire. We applied the added Lagrange method to describe the contact behavior between the rim and the tire. We meshed the geometric model of the tire section and pattern in Hypermesh and then assigned the corresponding material properties. We then imported the two meshed models into ABAQUS for component binding and spinning around the axis of symmetry to obtain the three-dimensional tire FEM with the surface pattern shown in Figure 1; the total number of elements is 223,452.

3.2. Asphalt Pavement Model. In this paper, the asphalt mixtures are AC, SMA, and OGFC, which are widely used as surface layers in asphalt pavement. Based on Chinese specifications [16], rutting slab specimens were made in the laboratory with a length and width of 300 mm and height of 50 mm; Table 1 presents the designed gradations for the three asphalt pavement types.

The pavement texture information for the asphalt concrete specimen was obtained by the X-ray tomography. 500 section images were acquired with a spacing of 0.1 mm, which met the accuracy requirements of the macroscopic texture. Then, the section images were noise reduced, enhanced, and binary processed with MATLAB; meanwhile, voids in asphalt mixtures were completely removed. Thus, each specimen FE model was extended to obtain the entire FEM of the asphalt concrete pavement with macrotexture information in ABAQUS, as shown in Figure 2.

3.3. Fluid Model. According to different reference coordinate systems, methods to establish a tire hydroplaning model can be divided into two categories: a tire rolling model and a flow model. The tire rolling model is more consistent with the actual working conditions of a tire, whereby the longitudinal displacement and circumferential displacement are imposed on the tire to make it roll forward on the road and keep the fluid static. The tire rolling over fluid in the model is used for tire hydroplaning analysis. As for the fluid model, the tire is rotated around the center axis and velocity is applied to the pavement and the fluid in the opposite direction to simulate the process of a tire rolling through water film.

For this study, we imposed the same load and displacement on the tire for the two modeling methods and calculated the flow traces under the tire extrusion, as shown in Figure 3. Compared to the flow model, we found that flow traces can be simulated completely by the tire rolling model. However, as the pavement model size increases, the computational efficiency decreases. The fluid model is easier to model with higher computation efficiency as well as better convergence compared to the tire rolling model. In this study, many tire models under high-speed motion are needed to be simulated, which required significant calculations. Thus, the proposed tire hydroplaning model is based on the flow model, not the rolling model.

We established the fluid model, which is composed of an air unit and a water unit, using ABAQUS/CAE. We adopted the Mie–Grüneisen equation of state to describe the mechanical responses and fluid characteristics of water film for a high-speed impact. We obtained the material parameters of the Mie–Grüneisen equation as $s = 1.92$ and $\Gamma_0 = 1.20$ based on Hugoniot [17] test data under the effect of fluid. For modeling fluid, the water is regarded as Newton fluid; that is, the fluid is incompressible. Based on the momentum conservation equation with which fluid complies and the Stokes equation, the Cauchy stress of fluid decomposes into shear stress and the surface pressure of the fluid microelement. Thus, the constitutive equation for the fluid model can be expressed as Equation (1). Using the model size of 80 mm × 390 mm × 320 mm, the mesh density is increased at the potential tire-pavement interface, and the minimum mesh size is 1 mm × 1 mm × 1 mm. The total number of EC3D8R Euler elements in the fluid is 381,420 and the node number is 415,576:

$$\rho_{\mathrm{w}}\left(\frac{\partial^{\mathrm{r}}_{u_i}}{\partial t} + {}^{\mathrm{r}}_{u_i} \cdot \nabla^{\mathrm{r}}_{u_i}\right) = -\nabla p + \eta \nabla^2 {}^{\mathrm{r}}_{u_i} + \rho_{\mathrm{w}} \mathbf{b}_{\mathrm{w}}, \tag{1}$$

where ρ_{w} is the fluid density, t is time, ${}^{\mathrm{r}}_{u_i}$ is the fluid velocity vector, p is the surface pressure of the microelement of water, η is the dynamic viscosity coefficient of fluid, and b_{w} is the volume gravity of the fluid.

3.4. CEL Method. As more stress and strain are produced that affect the ground and hydrodynamic pressure on a rolling tire, and thus affects the complex coupling dynamic deformation at tire and fluid interface, the CEL method can be applied to create grid divisions in the modeling process. The Lagrange unit is adopted to represent the inflated tire and the asphalt pavement, and the Euler unit is used to describe the turbulent fluid that is needed to build the model. We used speed to constrain the interface of these two units to ensure that the flow rate is coincident when different materials go through the mesh. Then, we calculated the interfacial stress values and iterated repeatedly until convergence occurred. We utilized generalized contact to define the effective contact between the two kinds of model units; Figure 4 presents the tire hydroplaning model.

The moving boundary of water film makes it difficult to determine the location of water film when a tire is rolling. Therefore, we applied a liquid surface tracking technique, or VOF [18], to simulate the movement of the fluid-tire interface in the tire hydroplaning model. In the VOF method, the Eulerian volume fraction f is defined by using the fluid through the element mesh, as expressed in Equation (2). The numerical value for function f represents the ratio of the fluid volume in the Eulerian elements to the whole Eulerian element and is the function of space and time:

$$\frac{\partial f}{\partial t} + v \nabla f = 0, \tag{2}$$

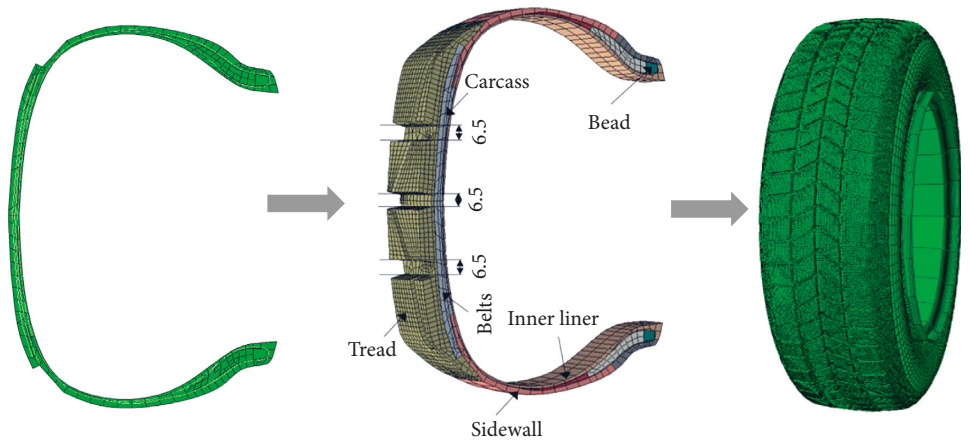

Figure 1: 3-D model of inflatable patterned tire.

Table 1: Design gradation of asphalt mixtures.

Components	Sieve size (mm) Passing rate of each sieve (%)									
	0.075	0.15	0.3	0.6	1.18	2.36	4.75	9.5	13.2	16
AC	6	10	13.5	19	26.5	37	53	76.5	95	100
SMA	10	13.2	16.3	19.5	22.7	25.8	29	63.5	97.9	100
OGFC	4.6	5.4	6.1	8.7	11.5	15.0	18.8	63.3	97.8	100

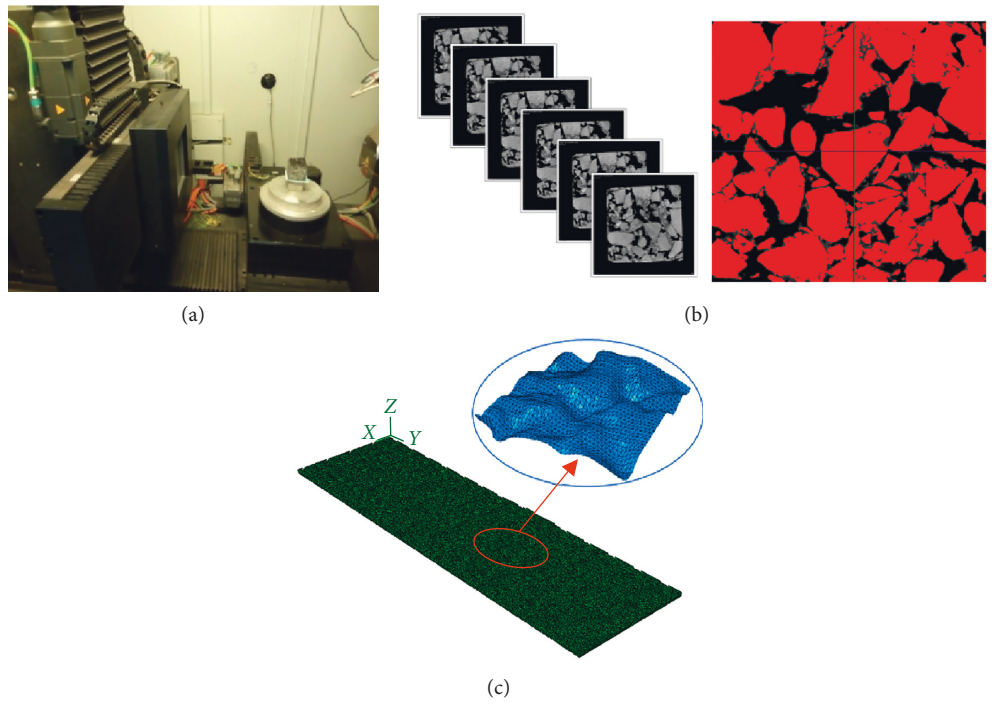

(a) (b) (c)

Figure 2: Procedures of modeling asphalt pavement: (a) scanning by the X-ray tomography; (b) threshold segmentation of the specimen images; (c) FE model of the asphalt pavement.

where v is the fluid velocity and t is the time. When $f = 1$, the mesh is filled with fluid; when $f = 0$, it is empty; and when $0 < f < 1$, the free surface exists in the mesh. Thus, the fluid free surface can be accurately described by this method.

In this paper, the temperature of the water film model is 20°C, its density is 998.2 kg/m^3, dynamic viscosity is 1.002×10^{-3} N·S/m^3, and the kinematic viscosity is 1.004×10^{-6} m^2/s.

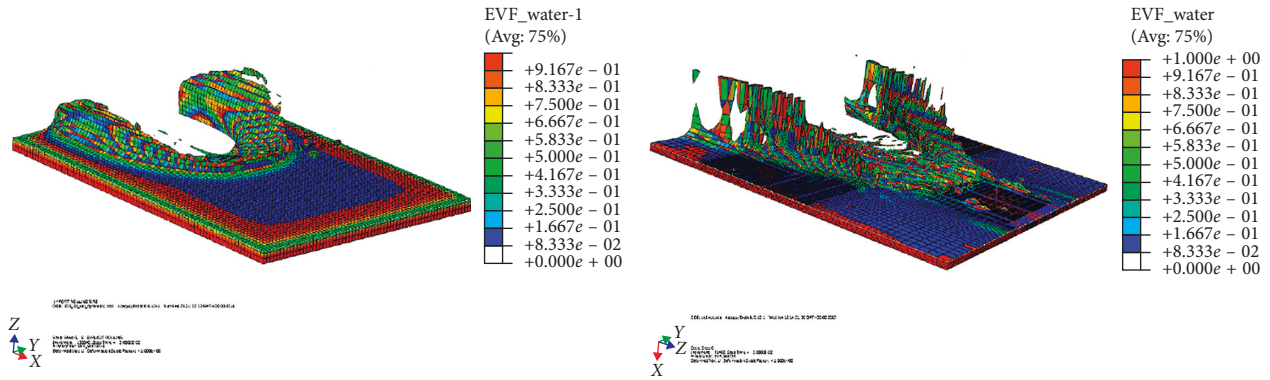

(a) (b)

Figure 3: Comparison of flow trace: (a) tire rolling model and (b) flow model.

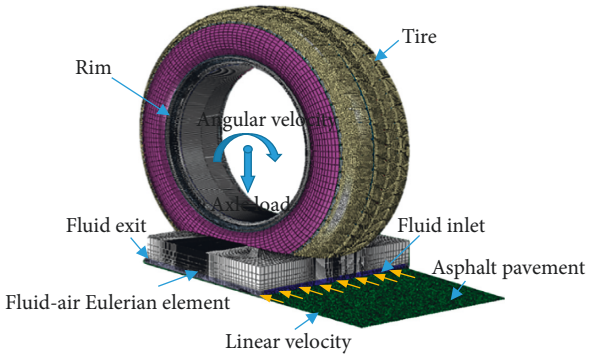

Figure 4: Components of the tire hydroplaning model.

3.5. Verification of the Tire Hydroplaning Model. In order to verify the applicability of the tire hydroplaning model, we validated the contact area of the tire-pavement interface. We set the tire speed at 70 km/h; the remaining boundary conditions were kept constant. Then, we analyzed the relationship between the tire-pavement contact area and the various stages in the hydroplaning process. As shown in Figure 5, the contact area with the tire rolling on dry asphalt pavement is the largest when the time is 7.003 s and the tire is gradually lifted off the pavement surface with continuous contact with the water. The tire-pavement contact area reached the balance state at $t = 7.020$ s. Figure 5 shows that the size of this area is a quarter of the initial contact area. The analysis results for the tire-pavement vertical contact force are consistent with those in the literature [19]. The results prove that the proposed tire hydroplaning model is effective for simulation.

4. Adhesion Coefficient of Tire-pavement Interface

Due to the effects of the tire pattern, road surface texture, and rubber material characteristics, the adhesion coefficient cannot be equal to the friction coefficient of the tire rubber material. The adhesion coefficient is the tangential force divided by the normal load. As the elastic slip only occurs and the driving wheel does not slip completely, a part of the tire-pavement contact area produces sliding friction. The contact area of the tire-pavement contains the adhesion region and the slipping region. The tangential reaction force on the tire is the sum of the longitudinal force in the adhesion region and the sliding friction in the slipping region [20, 21]. Hence, the adhesion coefficient can be calculated by

$$\mu = \frac{F_{xn} + F_{xb}}{F_h} < \mu_f, \tag{3}$$

where μ is the adhesion coefficient under dry condition, μ_f is the slipping friction coefficient, F_{xn} is the slipping friction in the adhesion region, and F_{xb} is the slipping friction in the slipping region (Figure 6).

The adhesion coefficient can be physically understood as the ratio of the sum of the tangential reaction forces acting on the contact surface to the normal load on the entire contact area. The adhesion coefficient is variable and gradually becomes larger with the increase of driving torque or braking torque applied to the tire, which does not follow Coulomb's law. When the slipping region is extended to the whole contact area, the adhesion is friction.

Asphalt pavement with a good surface macrotexture not only can improve the tire hydroplaning speed but also provide enough adhesion when the tire rolls over a wet surface. The friction coefficient between the tire tread rubber and the asphalt pavement under dry pavement conditions is defined based on the literature [22]. We adapted the tire hydroplaning model to calculate and analyze the adhesion coefficient for wet asphalt pavements under corresponding working conditions.

During the process of tire hydroplaning, the tire is forced via the axle load, the ground reaction force, and the fluid lift force in the vertical direction. However, in the horizontal direction, the tire can be subjected to the interaction of friction resistance between the road and the rubber, water flow impact force, fluid viscous force, etc. If the tire is assumed to roll in a straight line in the hydroplaning model, then factors such as lateral torque are not being considered in the model. Therefore, all horizontal resistance factors are collectively referred to as 'rolling resistance', as shown in Figure 7.

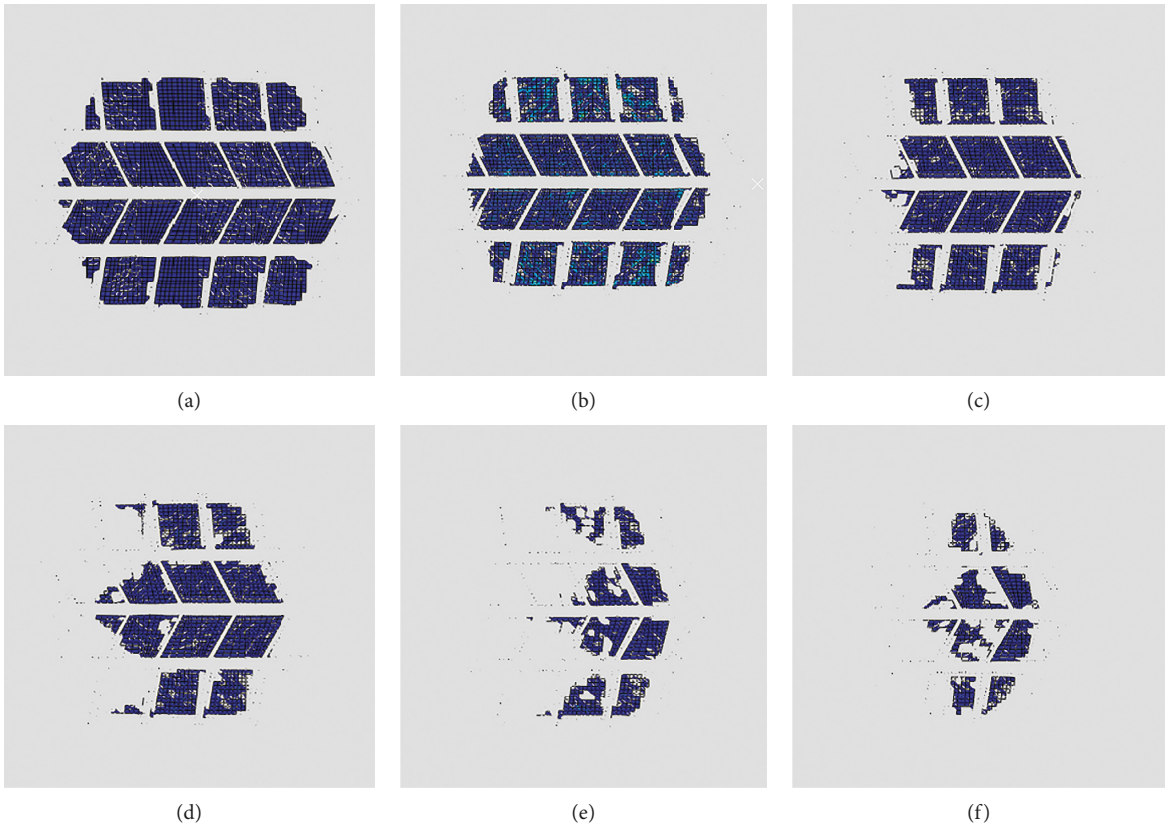

Figure 5: Footprint at tire-pavement interface in the process of tire hydroplaning: (a) $t = 7.003$ s; (b) $t = 7.005$ s; (c) $t = 7.007$ s; (d) $t = 7.010$ s; (e) $t = 7.015$ s; (f) $t = 7.020$ s.

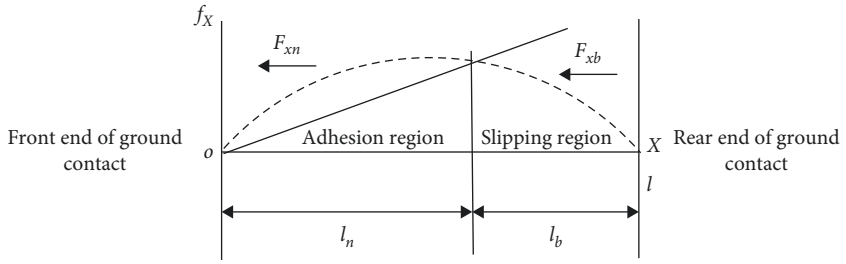

Figure 6: Schematic diagram of tire elastic slipping.

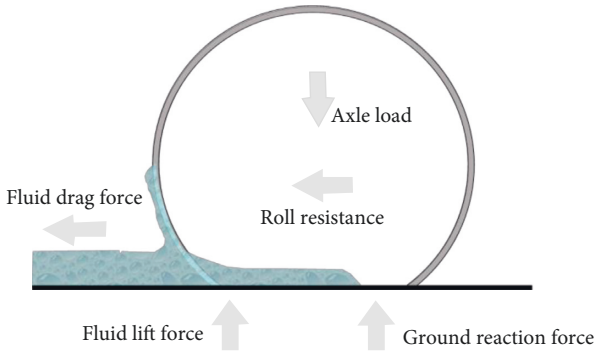

Figure 7: Force schematic during tire hydroplaning.

For the proposed hydroplaning model, Equation (4) is used to calculate the tire adhesion coefficient under wet conditions. In the model, the tire rolls in the Z direction, so the rolling resistance of the tire is calculated based on the joining force in the Z direction that is received by the reference point on the rim:

$$\mu_s = \frac{\mu\left(F_h - F_t\right) + F_{\mathrm{d}}}{F_h} = \frac{F_z}{F_h}, \tag{4}$$

where μ_s is the tire adhesion coefficient under wet conditions; μ is the tire adhesion coefficient under dry conditions; F_{d} is the fluid drag force; F_h is the tire axle load; F_z is the tire rolling resistance; and F_t is the fluid lift force.

When calculating the adhesion coefficient, a sufficiently long fluid model should be established on the asphalt pavement, and the force that the rim reference points experiences at the corresponding times in the horizontal direction is read to calculate the adhesion coefficient. Because the acceleration behavior of the tire on the water surface needs to be simulated, the inertial force should be applied to the fluid area to maintain the acceleration process of the water flow, and the rest of the boundary conditions must remain unchanged.

Given that vehicle tires brake from a pure rolling state to a locked position, and thus, the drag slip is a gradual process [23], we utilized the slip rate S to evaluate the proportion of wheel slippage. When the tire is braking, the speed of the wheel core is set as v and the rotational angular velocity is ω. Considering the equivalent radius r_e of the tire after vertical compression, the tire slip rate can be expressed as follows [24]:

$$S = \frac{(v - r_e\omega)}{v}. \tag{5}$$

Based on the three-dimensional FEM of a rolling tire, the vertical load of the wheel axle is kept constant. Using the same modeling process as the previous AC-13 pavement with macrotexture information, we established models for SMA-13 and OGFC-13, respectively. The tire longitudinal adhesion of the three types of asphalt pavement during braking was determined by adjusting the slip rate. With the specific normal force of the ground applied to the wheels, the braking longitudinal adhesion coefficient reaches its maximum when the slip rate is around 15 percent, which means that the adhesion between the tire and the pavement also is at its maximum, as shown in Figure 8(a). In addition, the braking effect confirms the theory that an antilock braking system (ABS) can shorten the vehicle braking distance. The braking effect provides the basis for analysis of the tire-pavement adhesion coefficient in the ABS state. When the slip ratio is greater than 15 percent, the longitudinal force decreases with an increase in the slip ratio; this outcome is caused by the relative sliding of the interface between the tire surface and the road surface, as shown in Figure 8(b).

5. Results and Discussion

In this study, we set the Eulerian fluid water film thickness in a three-dimensional inflatable patterned tire hydroplaning FEM to construct the tire and proposed pavement contact model. In accordance with the literature [25], we imported the rubber-pavement friction coefficient curve to the FE model and then analyzed the adhesion properties' influential factors of the tire-pavement interface under dry and wet conditions. To be well known, the adhesion coefficient of tire-pavement interface is affected by many factors, including vehicle factors (such as speed, slip ratio, camber, and axle load), tire factors (such as material, tire type, tire tread depth, and internal pressure), pavement factors (such as road type, macrotexture and microtexture, and drainage capacity), and road lubrication factors (such as lubricant type, depth, and temperature) [26]. For this study, we chose vehicle speed, tire inflation pressure, pavement macrotexture, and water film thickness as variables to analyze the change rule of the tire-pavement adhesion coefficient.

5.1. Influential Factors of Tire-Pavement Adhesion Coefficient at ABS State. When driving at a high speed on a dry road surface, the driver may make an emergency brake when encountering a sudden situation; then, the vehicle will automatically be in the ABS state. In order to determine the maximum safe speed when tires are hydroplaning under specific conditions, the tires need to be set at the ABS state. When the tire is in the ABS state, the contact behavior between the tread rubber and the pavement is complex. Therefore, the friction coefficient defined by traditional tribology theory is not suitable for evaluating tire skid resistance. In tire science, an adhesion coefficient as the value of the tangential force divided by the normal load is used.

In the ABS state, the user-defined friction model is applied. For this study, the axle load was set as 3922 N in the tire-pavement contact model; inflation pressures were set as 200 kPa, 240 kPa, 300 kPa, and 350 kPa, respectively, and the tire speeds were set at 40 km/h, 60 km/h, 80 km/h, and 100 km/h, respectively. The variation regulations of the tire adhesion coefficient with the inflation pressure, initial velocity, and MPD value were simulated in the ABS state, as shown in Figure 9.

Figure 9(a) shows that the tire adhesion coefficient increases with an increase in the tire inflation pressure, the overall change trend is parabolic, and the increasing amplitude decreases with an increase in inflation pressure. As the inflation pressure increases from 200 kPa to 240 kPa, the adhesion coefficient increases by 16 percent to 21 percent, the inflation pressure increases from 300 kPa to 350 kPa, and the adhesion coefficients increase by 8 percent to 10 percent, which is basically consistent with the test results of Goodyear Eagle tire. According to the field test results of Goodyear Eagle [27], the adhesion coefficient of tires with a pressure of 35 psi is greater than 24 psi as the vehicle speed is lower than 40 km/h. The difference may be caused by factors such as the material and structure of tire, the MPD value of asphalt pavement, etc. It is generally believed that the increase of tire inflation pressure will lead to the decrease of the adhesion coefficient. The effect of inflation pressure on the footprint contact area, slip ratio, tire rolling resistance, fluid lift, and drag forces will be discussed in detail in the next paper.

Figure 9(b) shows that, on the whole, the adhesion coefficient of the tire decreases gradually with an increase in driving speed. The tire adhesion coefficient for the AC pavement decreases by 21.3 percent with an increase in speed from 40 km/h to 100 km/h, for the SMA pavement decreases by 17.1 percent, and for the OGFC pavement decreases by 14.1 percent. Thus, with the increase in vehicle speed, the pavement with the best texture has superior skid resistance.

Six MPD values were considered in this study to further analyze the effects of asphalt pavement macrotexture on the tire adhesion coefficient; Figure 9(c) presents the calculation results. With an increase in the MPD value of the asphalt pavement, the tire adhesion coefficient also increases. This

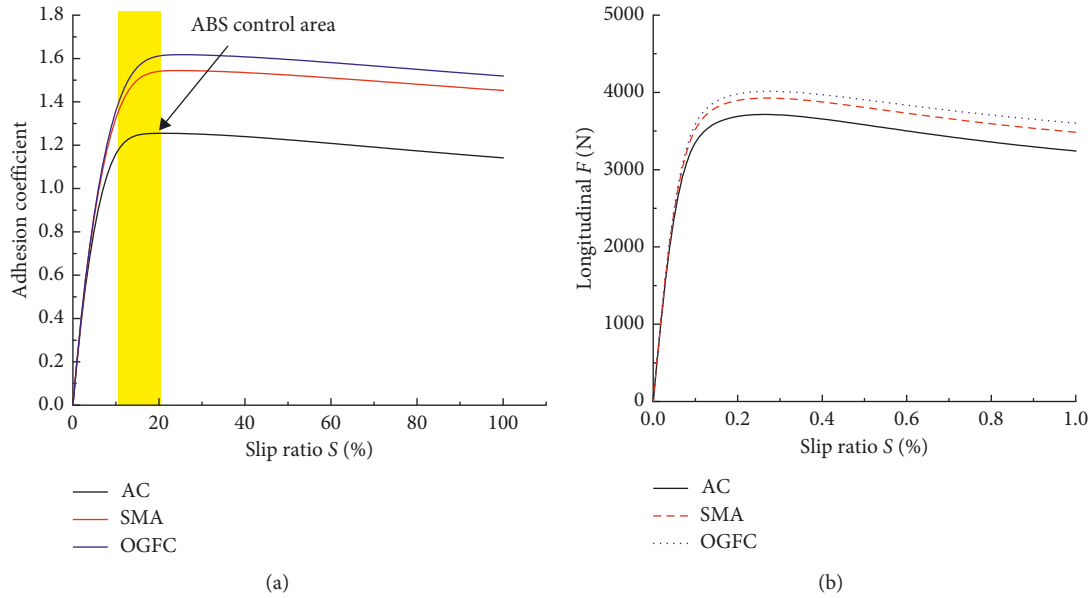

Figure 8: Adhesion characteristic curves of tire and pavement: (a) tire adhesion coefficient variation and (b) tire longitudinal force variation.

phenomenon is particularly obvious at a high-speed state. For example, when the asphalt pavement MPD value increases from 0.32 to 1.21 with a vehicle speed of 40 km/h, the adhesion coefficient increases by 33.7 percent; however, the adhesion coefficient increases by 47.1 percent when the velocity is 100 km/h.

5.2. Effect of Tire Speed on Adhesion Coefficient under Wet Conditions. In the inflation tire hydroplaning model, the tire inflation pressure is set at 240 kPa, the axle load is set at 3922 N, and the water film thicknesses are set as 2 mm and 5 mm, respectively. The adhesion coefficient for the three different asphalt pavements was analyzed with the tire speeds of 40 km/h, 60 km/h, 80 km/h, and 100 km/h, respectively. Figure 10 shows the effect of tire speed on the adhesion coefficient h_w representing the thickness of water film. The adhesion coefficient decreases with an increase in tire speed under all working conditions. However, the OGFC pavement has the highest adhesion coefficient with the same water film thickness and tire speed, followed by the SMA pavement, and the AC pavement has the lowest. With the same water film thickness, the adhesion coefficient of the AC pavement decreased by 15.4 percent with an increase in vehicle speed, the SMA pavement decreased by 11.8 percent, and the OGFC pavement decreased by 9.7 percent. The results show that the OGFC pavement with its open gradation design has better antiskid performance than the other graded asphalt pavements. In addition, for the same type of asphalt pavement, the water film with less thickness exhibits greater adhesion under the same driving speed, which is consistent with the phenomenon of hydroplaning when driving on rainy days.

5.3. Effect of Macrotexture on Adhesion Coefficient under Wet Conditions. In order to study the effects of different gradations of the same asphalt mixture type on pavement skid resistance, we adjusted the gradation of each type of asphalt mixture and obtained three rutting plates with different surface topographies. Macrotexture was selected as the evaluation index to analyze the effect of surface texture on the adhesion coefficient of the pavement. In view of the good correlation between the MPD and skid resistance of the tire, we used MATLAB to extract the MPD as the characteristic value for evaluating asphalt pavement macrotexture in this paper. We converted the mean texture depth (MTD) value (obtained by the sand patch method) to the MPD value according to the following equation from the international specification, ISO Part 2 [28]:

$$\text{MTD} = 0.8 \times \text{MPD} + 0.2. \quad (6)$$

By comparing the MPD values of the three types of pavement obtained from the sand patch method, as shown in Table 2, and with error less than 5 percent, we verified the accuracy of the MPD value via CT scanning. The tire inflation pressure was set at 240 kPa, the tire load was set at 3922 N, and the water film thicknesses were 2 mm and 5 mm, respectively. We established six pavement models with different macrotextures (MPD values of 0.32 mm, 0.47 mm, 0.63 mm, 0.83 mm, 1.01 mm, and 1.21 mm, respectively), to analyze the changing trend of the tire adhesion coefficient with increasing MPD of the pavement at the tire speeds of 20 km/h, 40 km/h, 60 km/h, 80 km/h, and 100 km/h, respectively.

Figure 11 shows that, for a constant water film thickness, the adhesion coefficient presents an increasing trend with an increase in the MPD at each speed, which is more obvious at higher tire speeds. When the thickness of the water film is 2 mm and the velocity is 20 km/h, the adhesion coefficient increases by 52.1 percent, and when the speed is 100 km/h, it increases by 67.9 percent. When the asphalt pavement has a high MPD value, increasing the speed leads to a decrease in the adhesion coefficient that is smaller than the low MPD value. That is, in this study, the adhesion coefficient reduced

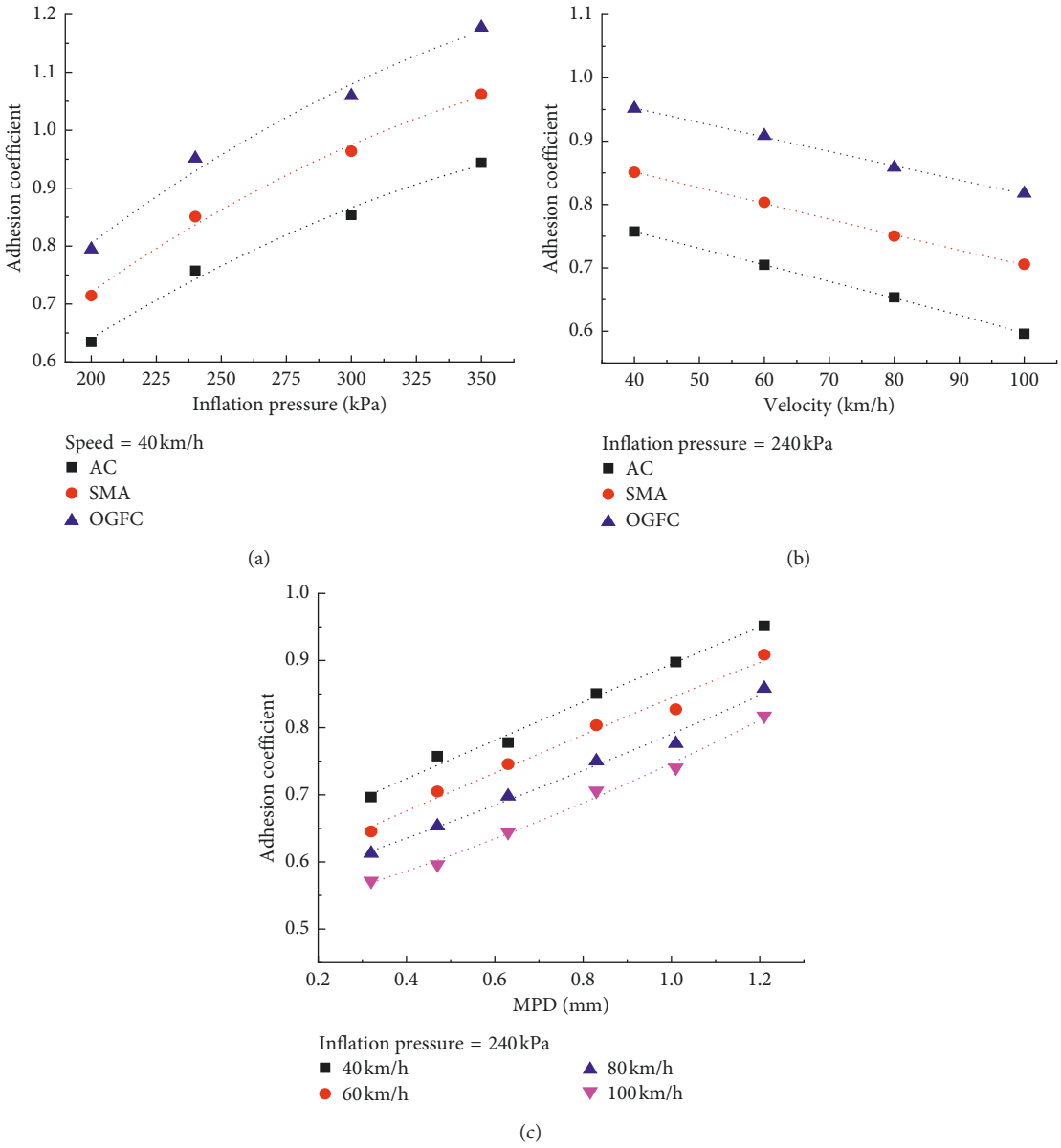

Figure 9: Influential factors analysis of the adhesion coefficient: (a) internal inflation pressure; (b) velocity; (c) MPD values.

by 14.8 percent when the vehicle speed was increased from 20 km/h to 100 km/h with the water film thickness of 2 mm and the MPD value of 0.32 mm, whereas when the MPD value was 1.21 mm and the other parameters were kept constant, the adhesion coefficient of the pavement reduced by 10.9 percent.

In summary, the higher the MPD value of an asphalt pavement, the greater the adhesion coefficient. When the MPD value is increased gradually, the increase in the adhesion coefficient is more obvious. In particular, the pavement shows better adhesion performance at the higher speeds.

6. Conclusions

In this study, we developed a FEM of a hydroplaning inflated tire using ABAQUS and according to three pavement surface topographies: AC, SMA, and OGFC pavements. We applied the CEL method and liquid surface tracking technique (VOF) to analyze the influential factors and change rules of the tire-pavement adhesion coefficient under dry and wet conditions. The main conclusions can be drawn as follows:

(i) The adhesion at a tire-pavement interface is related to the tire's moving state. With an increase in the slip rate, the longitudinal force of the tire first rises and then decreases. The longitudinal force reaches its maximum when the slip rate is about 15 percent. That slip rate is also the controlling slip rate for an ABS when the vehicle is braking in order to achieve greater braking force.

(ii) In the dry state (ABS), the tire friction coefficient increases with an increase in inflation pressure, and the overall trend presents a parabolic curve. This phenomenon indicates that high-inflation pressure

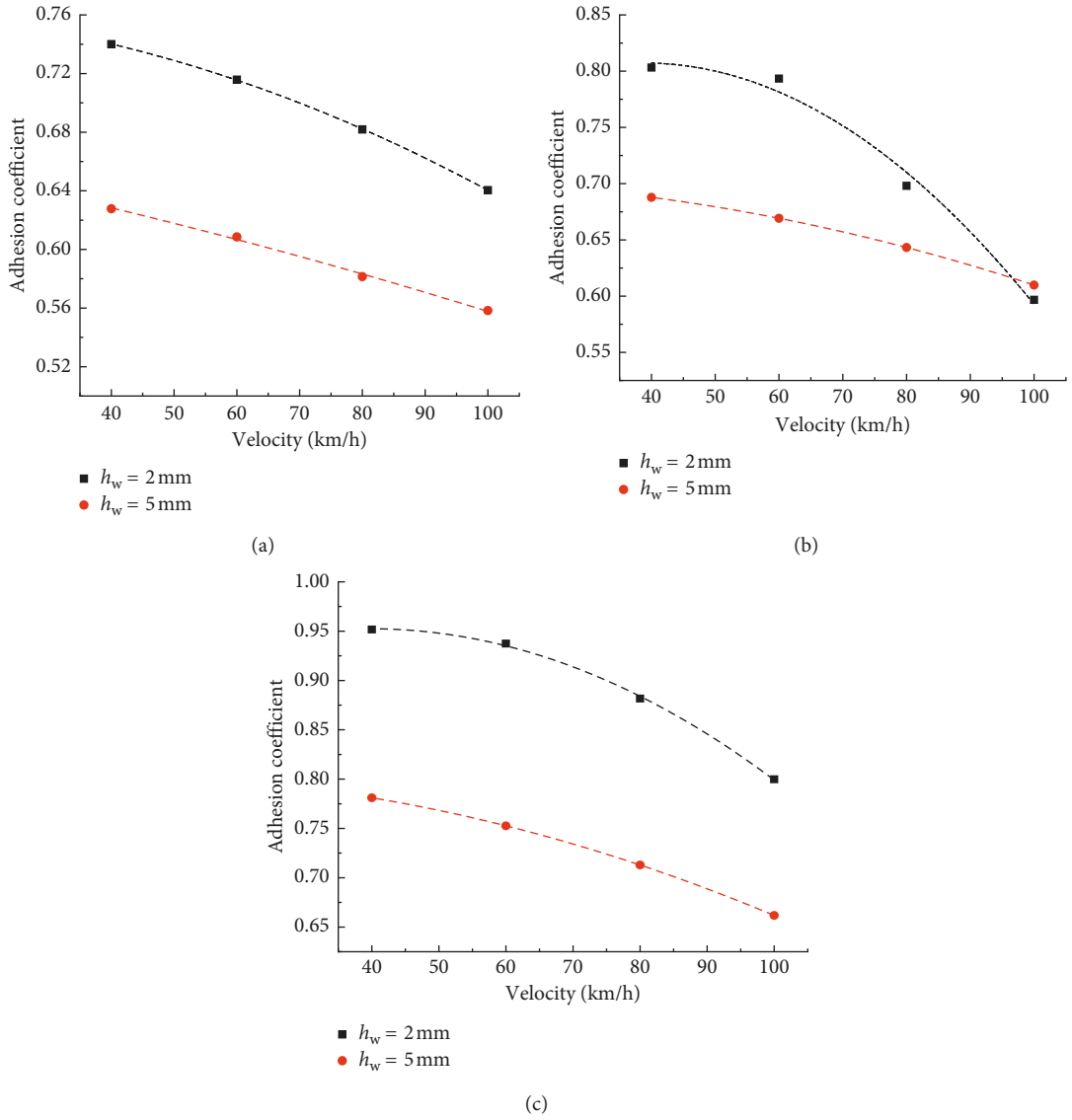

Figure 10: Variation curves of the adhesion coefficient with velocity: (a) AC pavement, (b) SMA pavement; (c) OGFC pavement.

Table 2: MPD values of three kinds of asphalt pavement.

Components	MTD values of sand patch method (mm)	MPD values converted (mm)	MPD values scanned (mm)	Error (%)
AC1	0.46	0.32	0.33	1.4
AC2	0.57	0.46	0.45	2.1
AC3	0.58	0.47	0.49	2.8
SMA1	0.71	0.63	0.65	3.1
SMA2	0.80	0.75	0.74	1.7
SMA3	0.86	0.83	0.85	2.5
OGFC1	1.02	1.01	0.99	1.6
OGFC2	1.04	1.05	1.08	2.7
OGFC3	1.17	1.21	1.17	2.9

helps us to improve the tire's skid resistance. The friction coefficient of the tire decreases gradually with an increase in driving speed; the adhesion coefficient of the AC pavement decreases the most of all the pavements, by 21.3 percent, indicating that higher speeds have serious negative impacts on traffic safety. When the MPD value increases from 0.32 to 1.21, the adhesion coefficient increases by 33.7 percent, which illustrates that the higher the MPD value of the asphalt pavement, the greater the tire adhesion coefficient, especially under high-speed conditions.

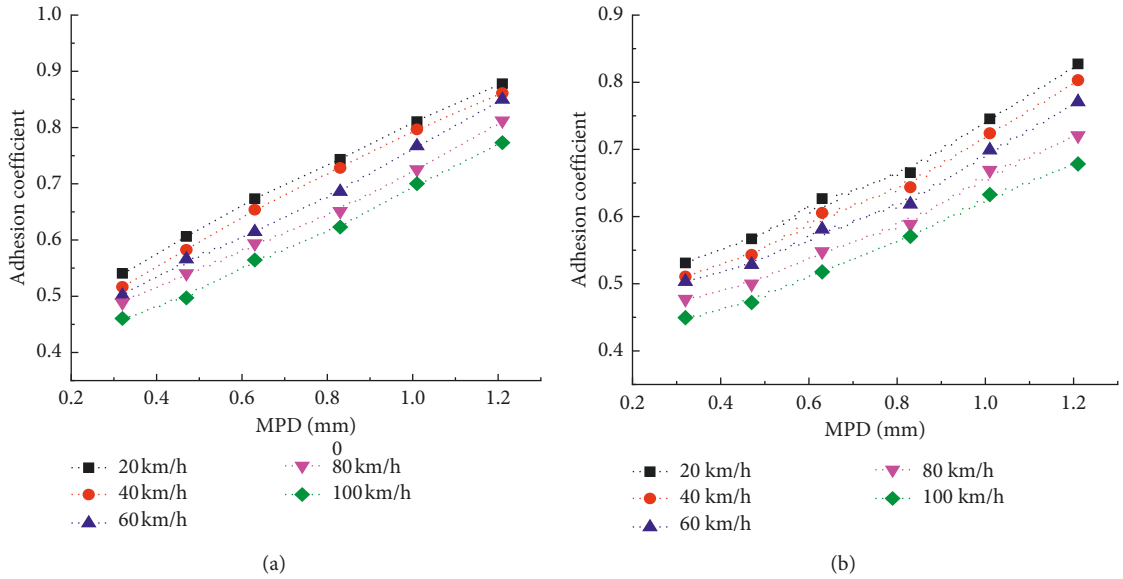

Figure 11: Variation of the adhesion coefficient with the MPD value: (a) 2 mm of water film thickness; (b) 5 mm of water film thickness.

(iii) Under wet pavement conditions, high tire inflation pressure can effectively improve the tire hydroplaning speed. The increase in the amplitude of the hydroplaning tire speed decreases gradually with an increase in the surface water film thickness. The tire hydroplaning speeds on different pavements are ranked as OGFC > SMA > AC. With gradually increasing speed, the adhesion coefficient of the OGFC pavement decreased the least, by 9.7 percent. The adhesion coefficient increases with an increase in the MPD at each speed with a specific water film thickness. Simultaneously, with an increase in MPD value, the decrease in the amplitude of the adhesion coefficient lessens with an increase in velocity. When the MPD value improves from 0.32 to 1.21, the adhesion coefficient of the asphalt pavement increases by 26.2 percent.

(iv) With certain water film thicknesses, the adhesion coefficient decreases with an increase in vehicle speed; the OGFC pavement showed the highest adhesion property, followed by the SMA pavement and then the AC pavement. This outcome indicates that the OGFC pavement that is designed with open gradation has better skid resistance than the other gradation designs when the driving speed increases with a constant water film thickness. For the same asphalt pavement macrotexture, the adhesion coefficient of the dry pavement is higher than that of the wet conditions.

7. Future Work

For this paper, we analyzed only typical factors (pavement materials, tire inflation pressure, tire speed, water film thickness, and pavement macrotexture) and did not consider other factors such as tire type, tire tread depth, pavement drainage capacity, and road lubrication factors (lubricant type and temperature) that may affect tire-pavement adhesion properties. Therefore, various tire types with different tread patterns, different pavement drainage capacities, and different road temperatures should be considered in future work.

Although the results obtained in this study provide new insights for designing asphalt pavements with good skid resistance, a further study is required to evaluate the effects of pavement macrotexture on potential damage to tires and the brake performance of an automated vehicle. In addition, the definition of actual water film thickness and the effects of rainwater seepage into porous pavement on the adhesion coefficient of the tire-pavement interface also should be considered in rainy regions.

Data Availability

Previously reported data were used to support this study and are available at DOI: 10.1155/2017/5843061. These prior studies (and datasets) are cited at relevant places within the text as references [19, 25].

Conflicts of Interest

The authors declare that they have no conflicts of interest regarding the publication of this paper.

Acknowledgments

The study is financially supported by the National Natural Science Foundation of China (No. 51778139), and Scientific Research Innovation Project of Jiangsu Province in China (No. KYCX18_0146), and Fundamental Research Funds of the Central Universities (No. 2242017K401).

References

[1] T. Ji, X. Huang, and Q. Liu, "Part hydroplaning effect on pavement friction coefficient," *Journal of Traffic and Transportation Engineering*, vol. 3, no. 4, pp. 9–12, 2003.

[2] F. Duarte, A. Ferreira, P. Fael et al., "Software tool for simulation of vehicle - road interaction," *Engineering Computations*, vol. 34, no. 5, pp. 1501–1526, 2017.

[3] E. R. Jones and R. L. Childers, *Contemporary College Physics*, Addison-Wesley Pub. Co, Boston, MA, USA, 1993.

[4] G. Gim, "An analytical model of pneumatic tyres for vehicle dynamic simulations, part 1: pure slips," *International Journal Vehicle Design*, vol. 11, no. 6, pp. 589–618, 1990.

[5] H. P. Dugoff, P. S. Fancher, and L. Segel, "An analysis of tire traction properties and their influence on vehicle dynamic performance," in *Proceedings of International Automobile Safety Conference*, SAE Technical Paper 700377, vol. 79, pp. 1–25, New York, NY, USA, 1970.

[6] C. C. De Wit, H. Olsson, K. J. Astrom, and P. Lischinsky, "A new model for control of systems with friction," *IEEE Transactions on Automatic Control*, vol. 40, no. 3, pp. 419–425, 1995.

[7] S. Germann, M. Wurtenberger, and A. Daiss, "Monitoring of the friction coefficient between tire and road surface," in *Proceedings of the Third IEEE Conference on Control Applications, IEEE*, vol. 1, pp. 613–618, 1994.

[8] H. B. Pacejka and E. bakker, "The magic formula tire model," *Vehicle System Dynamics*, vol. 21, no. 1, pp. 1–18, 1992.

[9] G. P. Ong and T. F. Fwa, "A mechanistic interpretation of braking distance specifications and pavement friction requirements," *Transportation Research Record: Journal of the Transportation Research Board*, vol. 2155, no. 1, pp. 145–157, 2010.

[10] T. F. Fwa, H. R. Pasindu, and G. P. Ong, "Critical rut depth for pavement maintenance based on vehicle skidding and hydroplaning consideration," *Journal of Transportation Engineering*, vol. 138, no. 4, pp. 423–429, 2012.

[11] F. Ju, T. F. Fwa, and G. P. Ong, "Evaluating wet weather driving benefits of grooved pavements," *International Journal of Pavement Research and Technology*, vol. 6, no. 4, pp. 287–293, 2013.

[12] H. R. Pasindu and T. F. Fwa, "Improving wet-weather runway performance using trapezoidal grooving design," *Transportation in Developing Economies*, vol. 1, no. 1, pp. 1–10, 2015.

[13] B. Chen, X. Zhang, J. Yu et al., "Impact of contact stress distribution on skid resistance of asphalt pavements," *Construction and Building Materials*, vol. 133, pp. 330–339, 2017.

[14] F. Gustafsson, "Estimation and change detection of tire-road friction using the wheel slip," in *Proceedings of the 1996 IEEE International Symposium On Computer-Aided Control System Design*, pp. 99–104, Dearborn, MI, USA, 1996.

[15] S. Zhu and X. Huang, "Numerical simulation of tire critical hydroplaning speed on transverse grooved concrete pavement," *Journal of Southeast University (Natural Science Edition)*, vol. 46, no. 6, pp. 1296–1300, 2016.

[16] M. O. T. O., "China, standard test methods of bitumen and bituminous mixtures for highway engineering," *JTG E20-2011*, China Communications Press, China, 2011.

[17] K. Anupam, "Numerical simulation of vehicle hydroplaning and skid resistance on grooved pavement," National University of Singapore: doctoral thesis, 2012.

[18] B. Li, *Study on the Surface Functions for Grooved Concrete Pavement*, School of Transportation, Chang'an University, Xi'an, China, 2011.

[19] X. Liu, Q. Cao, and S. Zhu, "Numerical simulation of tire critical hydroplaning speed on asphalt pavement," *Journal of Southeast University (Natural Science Edition)*, vol. 47, no. 5, pp. 1020–1025, 2017.

[20] J. Zhuang, *Vehicle Tire Mechanics*, Beijing Institute of Technology Press, Beijing, China, 2009.

[21] J. R. Barber, "Contact mechanics," *Solid Mechanics and Its Applications*, Springer International Publishing, Basel, Switzerland, 2018.

[22] B. N. J. Persson, "Theory of rubber friction and contact mechanics," *Journal of Chemical Physics*, vol. 115, no. 8, pp. 3840–3861, 2001.

[23] K. Guo, "Unitire: unified tire model," *Chinese Journal of Mechanical Engineering*, vol. 52, no. 12, pp. 90–99, 2016.

[24] B. N. Persson, "Rubber friction and tire dynamics," *Journal of Physics: Condensed Matter*, vol. 23, no. 1, article 015003, 2011.

[25] S. Zhu, X. Liu, and Q. Cao, "Numerical study of tire hydroplaning based on power spectrum of asphalt pavement and kinetic friction coefficient," *Advances in Materials Science and Engineering*, vol. 2017, Article ID 5843061, 11 pages, 2017.

[26] T. Bachmann, *Wechselwirkungen Im Prozeß Der Reibung Zwischen Reifen Und Fahrbahn, Deutsch*, 1998.

[27] U.S. Department of Transportation (USDOT), *Research and Innovative Technology Administration, Bureau of Transportation Statistics, Highlights of the 2001 National Household Travel Survey*, Bureau of Transportation Statistics, Washington, DC, USA, 2003.

[28] International Organization for Standardization, BS EN ISO 13473-2:2002(E), *Characterization of pavement texture by use of surface profiles-Part 2: Terminology and basic requirements related to pavement texture profile analysis*, International Organization for Standardization, 2002.